Model Hamiltonian for topological Kondo insulator SmB_6

Rui Yu[1], HongMing Weng[2,3], Xiao Hu[1], Zhong Fang[2,3] and Xi Dai[2,3]
[1] *International Center for Materials Nanoarchitectonics (WPI-MANA), National Institute for Materials Science, Tsukuba 305-0044, Japan*
[2] *Beijing National Laboratory for Condensed Matter Physics, and Institute of Physics,Chinese Academy of Sciences, Beijing 100190, China and*
[3] *Collaborative Innovation Center of Quantum Matter, Beijing 100190, China**
(Dated: June 30, 2014)

Starting from the k·p method in combination with first-principles calculations, we systematically derive the effective Hamiltonians that capture the low energy band structures of recently discovered topological Kondo insulator SmB_6. Using these effective Hamiltonians we can obtain both the energy dispersion and the spin texture of the topological surface states, which can be detected by further experiments.

PACS numbers: 73.43.-f, 73.22.-f, 71.70.Ej, 85.75.-d

arXiv:1406.7055v1 [cond-mat.mtrl-sci] 27 Jun 2014

I. INTRODUCTION

Searching for new topological insulators (TI) has become an active research field in condensed matter physics[1,2]. A topological insulator has insulating and topologically non-trivial bulk band structure giving rise to robust Dirac like surface states, which are protected by time reversal symmetry and have the spin-momentum locking feature. Such topological surface states have several remarkable properties. For example, the suppression of back scattering and localization on the TI surface[3–7]. Furthermore, if superconductivity is induced on the surface of TIs via proximity effects, the Majorana bound states can be induced[8–10]. These novel properties make topological insulator a promising platform for the design of spintronics devices and future quantum computing applications[11].

Recently the mixed valence compound SmB_6 has been proposed to be topological insulator and attracts lots of research interests[12–17]. Unlike the other well studied topological insulator materials, i.e. the Bi_2Se_3 family, the strong correlation effects in mixed valence TIs are crucial to understand the electronic structure due to the partially filled 4f bands[17–19]. There are two main effects induced by the on-site Coulomb interaction among the f-electrons, one is the strong modification of the 4f band width, the other is the correction to the effective spin-orbital coupling and crystal field[20–22]. As a consequence, the band inversion in the modified band structure happens between the 5d and 4f band (with total angular momentum j=5/2) around the three X points in the Brillouin Zone. Unlike the situation in Bi_2Se_3 family, where the band inversion happens between two bands both with the p character and similar band width, the band inversion in SmB_6 happens between two bands with the band widths differing by orders, which leads to very unique low energy electronic structure. Since the band inversion happens at the Zone boundary (X points), which project to three different points in surface Brillouin Zone leading to three different Dirac points on generic surfaces.

Experimentally, the first evidence of topological surface states has been found by transport measurements, and then by angle resolved photo emission spectroscopy (ARPES), Scanning Tunneling Spectroscopy (STS), quantum oscillation magneto-resistance measurements[23–35]. Unlike the electronic structures in large energy scale, which is mainly determined by the local atomic physics, the topological nature of the electronic structure can be fully described by the quasi-particle structure only, whose form can be determined from the symmetry principles. In the present paper, we will construct a k·p model capturing the full topological and symmetry features of the low energy quasi-particle structure, which leads to topological surface states with the renormalized Fermi velocities. All the symmetry allowed terms in the above k·p model have been obtained by fitting with the band structure obtained by the LDA+Gutzwiller calculation introduced in a previous paper[17]. Such a analytical model gives a clear theoretical description for the quasi-particle structure of SmB_6, which can be widely used in the further studies.

The organization of the present paper is as follows. In Sec.II, we present the crystal structure and band structure of SmB_6. Then we construct the effective models to describe the bulk band structure for this material from the symmetry considerations in Sec.III. Furthermore we calculate surface states and the spin texture on the the (001) surface based on our model Hamiltonian and show that it is consistent with the tight-binding calculation results. Conclusions are given in the end of this paper.

II. CRYSTAL STRUCTURE AND BAND STRUCTURE

In this section we first describe the crystal structure of the SmB_6 and then discuss the nontrivial topological bulk band structure of it.

crystal structure: SmB_6 has the CsCl-type crystal structure with $Pm\bar{3}m$ space group. The Sm ions are located at the corner and B_6 octahedron are located at the body center of the cubic lattice as shown in Fig-

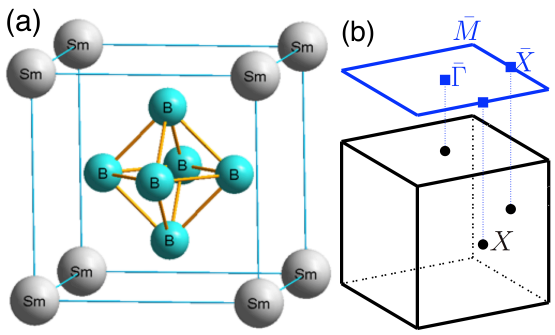

FIG. 1. (Color online) (a) The CsCl-type structure of $SmB_6$with $Pm\bar{3}m$ space group. Sm ions and B_6 octahedron are located at the corner and center of the cubic lattice respectively. (b) The bulk Brillouin zone of SmB_6 (black cubic) and its projection onto the (001) (blue square). The X points (black dots) in the bulk BZ are projected to $\bar{\Gamma}$ and $\bar{X}$ points (blue square points) in the (001) surface BZ.

ure 1(a). The corresponding bulk and projected Brillouin zone (BZ) of (001) surface for SmB_6 are shown in Fig.1(b).

electronic structure: Previous electronic structure studies find that in SmB_6 the band inversion happens between Sm 4f bands with total angular momentum $j = 5/2$ and one of the 5d bands, which leads to fractional occupation in 4f $j = 5/2$ orbitals or "non-integer chemical valence"[36–39]. Since the band inversion happens at three X points in the BZ, where the 4f and 5d states have opposite parities, the Z_2 topological nontrivial band structure is formed[40,41]. In order to include the strong Coulomb interaction among the f electrons, we implement the local density approximation in density functional theory with the Gutzwiller variational method (LDA+Gutzwiller) and apply it to calculate the renormalized band structure of SmB_6.

Here we briefly introduce the LDA+Gutzwiller method, for detailed descriptions please refer to Ref.[17 and 42]. The LDA+Gutzwiller method combines the LDA with Gutzwiller variational method, which takes care of the strong atomic feature of the f-orbitals in the ground state wave function. In this method, we implement the single particle Hamiltonian obtained by LDA with on site interaction terms describing the atomic multiplet features, which can be written as,

$$H = H_{LDA} + H_{int} + H_{DC} \tag{1}$$

where H_{LDA}, H_{int} and H_{DC} represent the LDA Hamiltonian, on-site interaction and the double counting terms respectively[43]. The LDA Hamiltonian can be expressed in a tight binding form by constructing the projected Wannier functions for both 5d and 4f bands[44–46].The on-site interactions can be described in terms of Slater integrals as introduced in detail in the previous paper[17]. The double counting term H_{DC} subtracts the correlation energy already included in LDA calculation. Within the Gutzwiller approximation, an effective Hamiltonian H_{eff} describing the quasi-particle band structure can be obtained, which describes the low energy dynamics including the topological surface states[17]. To further study the low energy physics of SmB_6, i.e. the behavior of the surface states, a simple k·p model Hamiltonian will be very useful. In the next section, we will construct such a model by expanding the H_{eff} near the three X points.

III. MODEL HAMILTONIAN FOR SMB_6

In this section, we will systematically derive the effective Hamiltonian near X points based on k·p theory combined with the results of first-principle calculations. We only give the effective Hamiltonian at $X_1 = (0, 0, \frac{1}{2})$ point. The effective Hamiltonian at the other two X points can be obtained by acting C_{4x} or C_{4y} rotation operations on the Hamiltonian at X_1. Using the symmetry group at the X point we can construct the effective k·p model near this point and all the parameters used in such a model can be obtained by fitting to the renormalized band structure obtained by LDA+Gutzwiller.

The k·p Hamiltonian is obtained from our one-partial effective Hamiltonian

$$H_{eff}\psi_{n,\mathbf{k}}(\mathbf{r}) = E_{n,\mathbf{k}}\psi_{n,\mathbf{k}}(\mathbf{r}), \tag{2}$$

where $\psi_{n,\mathbf{k}} = e^{i\mathbf{k}\cdot\mathbf{r}}u_{n,\mathbf{k}}(\mathbf{r})$ are the Bloch wave functions and the effective Hamiltonian only consists of the kinetic-energy operator, a local periodic crystal potential, and the spin-orbit interaction term:

$$H_{eff} = \frac{p^2}{2m} + V(\mathbf{r}) + \frac{\hbar}{4m_0^2c^2}(\sigma \times \nabla V)\cdot\mathbf{p}. \tag{3}$$

In terms of the cellular functions $u_{n,\mathbf{k}}(\mathbf{r})$, Eq.(2) becomes

$$H_{\mathbf{k}}u_{n,\mathbf{k}}(\mathbf{r}) \equiv \left[\frac{p^2}{2m} + V(\mathbf{r}) + \frac{\hbar}{4m_0^2c^2}(\sigma \times \nabla V)\cdot(\mathbf{p} + \hbar\mathbf{k}) + \frac{\hbar}{m}\mathbf{k}\cdot\mathbf{p}\right]u_{n,\mathbf{k}}(\mathbf{r}) = \epsilon_{n,\mathbf{k}}u_{n,\mathbf{k}}(\mathbf{r}), \tag{4}$$

where $\epsilon_{n,\mathbf{k}} \equiv E_{n,\mathbf{k}} - \frac{\hbar^2k^2}{2m}$. Expanding the above Hamiltonian at given high symmetry point k_0, the eigen-equation at $k_0 + k$ can be obtained by

$$\left[H_{\mathbf{k}_0} + \frac{\hbar}{m}\mathbf{k}\cdot\mathbf{p}\right]u_{n,\mathbf{k}_0+\mathbf{k}}(\mathbf{r}) = \epsilon_{n,\mathbf{k}_0+\mathbf{k}}u_{n,\mathbf{k}_0+\mathbf{k}}(\mathbf{r}), \tag{5}$$

where we have ignored the k-dependent spin-orbit term, which is usually much small. Once $E_{n,\mathbf{k}_0}$ and $u_{n,\mathbf{k}_0}$are known, the function $u_{n,\mathbf{k}_0+\mathbf{k}}(\mathbf{r})$ can be obtained by treating the term $H_{kp} = \frac{\hbar}{m}\mathbf{k}\cdot\mathbf{p}$ in Eq.(5) as a perturbation. It is more convenient to rewrite the perturbation as

$$H_{kp} = \frac{\hbar}{m}\mathbf{k}\cdot\mathbf{p} = \frac{\hbar}{2m}(k_+p_- + k_-p_+) + \frac{\hbar}{m}k_zp_z, \tag{6}$$

where the operator $p_\pm = p_x \pm ip_y$ and $k_\pm = k_x \pm ik_y$.

In the SmB_6 system, we expand the H_{eff} near the three X points. We chose the k·p basis function at X point as

$$\left|\frac{3}{2},\frac{3}{2}\right\rangle_d, \left|\frac{3}{2},-\frac{3}{2}\right\rangle_d, \left|\frac{5}{2},\frac{5}{2}\right\rangle_f, \left|\frac{5}{2},-\frac{5}{2}\right\rangle_f$$
$$\left|\frac{5}{2},\frac{3}{2}\right\rangle_f, \left|\frac{5}{2},-\frac{3}{2}\right\rangle_f, \left|\frac{5}{2},\frac{1}{2}\right\rangle_f, \left|\frac{5}{2},-\frac{1}{2}\right\rangle_f, \quad (7)$$

which can well describe the orbital characters for the eigenstates near the Fermi energy. We can then project the k·p Hamiltonian into above basis and the matrix elements of H_{kp} are constrained by the crystal symmetries at X point. The little group at X point is D_{4h}, which contains the following symmetry operations:

(1) fourfold rotation along the z direction $\hat{C}_{4z}$ $=e^{-i\frac{2\pi}{4}\hat{J}_z}$, where $\hat{J}_\alpha$ $(\alpha = x, y, z)$ is the operator for the α component of the total angular momentum.

(2) inversion symmetry $\hat{P} = I_2 \oplus -I_6$, where I_m is the m×m identity matrix.

(3) time reversal symmetry $\hat{T}$=$\Theta K = e^{-i\pi\hat{J}_y}K$, where K is the complex conjugate operator.

(4) twofold rotation along y direction $\hat{C}_{2y} = e^{-i\pi\hat{J}_y}$.

The symmetry operation can help us to reduce the independent parameters that appear in the $k \cdot p$ Hamiltonian. For example, considering the rotation C_{4z} around the z direction, we have

$${}_d\left\langle\frac{3}{2},\frac{3}{2}\right| p_- \left|\frac{5}{2},\frac{5}{2}\right\rangle_f = {}_d\left\langle\frac{3}{2},\frac{3}{2}\right| C_{4z}^\dagger C_{4z} p_- C_{4z}^\dagger C_{4z} \left|\frac{5}{2},\frac{5}{2}\right\rangle_f . \quad (8)$$

Since ${}_d\langle\frac{3}{2},\frac{3}{2}|C_{4z}^\dagger = {}_d\langle\frac{3}{2},\frac{3}{2}|e^{i\frac{2\pi}{4}\frac{3}{2}}$, $C_{4z}p_\pm C_{4z}^\dagger = e^{\mp i\frac{2\pi}{4}}p_\pm$, and $C_{4z}|\frac{5}{2},\frac{5}{2}\rangle_f = e^{-i\frac{2\pi}{4}\frac{5}{2}}|\frac{5}{2},\frac{5}{2}\rangle_f$, we get that $c_1 \equiv \frac{\hbar}{2m}{}_d\langle\frac{3}{2},\frac{3}{2}|p_-|\frac{5}{2},\frac{5}{2}\rangle_f$ is invariant under C_{4z} rotation and can be non-zero. While ${}_d\langle\frac{3}{2},\frac{3}{2}|p_+|\frac{5}{2},\frac{5}{2}\rangle_f$ get a minus sign under C_{4z} rotation, which means it must vanish. Following the same procedge, we can get $c_1' \equiv \frac{\hbar}{2m}{}_d\langle\frac{3}{2},-\frac{3}{2}|p_+|\frac{5}{2},-\frac{5}{2}\rangle_f$ is finite. When considering the 2-fold rotation along the y direction C_{2y}, we get the relation between c_1 and c_1' as

$$\begin{aligned} c_1 &= \frac{\hbar}{2m}{}_d\langle\frac{3}{2},\frac{3}{2}|p_-|\frac{5}{2},\frac{5}{2}\rangle_f \\ &= \frac{\hbar}{2m}{}_d\langle\frac{3}{2},\frac{3}{2}|C_{2y}^\dagger C_{2y} p_- C_{2y}^\dagger C_{2y}|\frac{5}{2},\frac{5}{2}\rangle_f \\ &= -\frac{\hbar}{2m}{}_d\langle\frac{3}{2},-\frac{3}{2}|p_+|\frac{5}{2},-\frac{5}{2}\rangle_f = -c_1'. \end{aligned} \quad (9)$$

Due to the time-reversal symmetry, the c_1 can be chosen to be real. Similar considerations can be used to calculate all matrix elements and we obtain the effective Hamiltonian, which is invariant under all symmetry operations

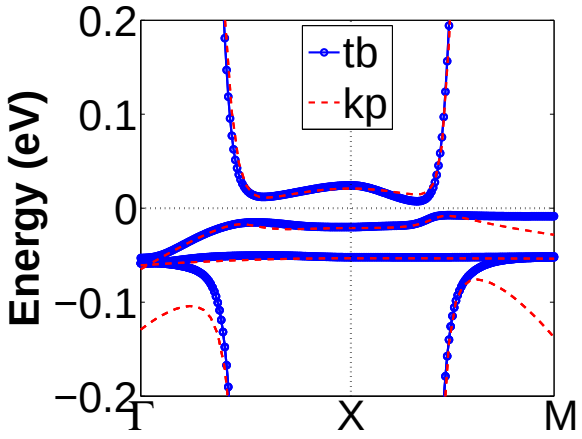

FIG. 2. The energy dispersion obtained from our model Hamiltonian with 8 bands (thin red line) is compared with that from tight-binding calculations (thick blue line). Here M to X lines represents the dispersion along the k_x direction while the X to Γ lines is for the k_z direction..

at X point up to the first order of k,

$$H_X = \begin{pmatrix} \epsilon_d & 0 & c_1k_+ & c_2k_z & c_3k_z & c_4k_+ & c_5k_- & 0 \\ & \epsilon_d & c_2k_z & -c_1k_- & -c_4k_- & c_3k_z & 0 & -c_5k_+ \\ & & \epsilon_{f_5} & 0 & 0 & d_1 & 0 & 0 \\ & & & \epsilon_{f_5} & d_1 & 0 & 0 & 0 \\ & & & & \epsilon_{f_3} & 0 & 0 & 0 \\ & & \dagger & & & \epsilon_{f_3} & 0 & 0 \\ & & & & & & \epsilon_{f_1} & 0 \\ & & & & & & & \epsilon_{f_1} \end{pmatrix}, \quad (10)$$

where $\epsilon_d = D + D_{xy}(k_x^2+k_y^2) + D_z k_z^2$, $\epsilon_{f_i} = F_i + F_{i,xy}(k_x^2+k_y^2) + F_{i,z}k_z^2$ $(i = 5, 3, 1)$ and $k_\pm = k_x \pm ik_y$. The parameters are listed in Table.I. The fitted energy dispersion for SmB_6 is plotted in Fig.2. It shows that our model Hamiltonian with eight bands captures the main features of the band dispersion near X point.

TABLE I. Parameters in our model Hamiltonian fitted for SmB_6, where the unit of energy is eV and the unit of length is the lattice constant.

D	D_{xy}	D_z	F_1	$F_{1,xy}$	$F_{1,z}$
-1.5698	29.9233	18.2502	-0.0532	-0.0020	-0.0300
F_3	$F_{3,xy}$	$F_{3,z}$	F_5	$F_{5,xy}$	$F_{5,z}$
0.0163	-0.5776	-0.4476	-0.0164	-0.1543	-0.1543
c_1	c_2	c_3	c_4	c_5	d_1
-0.2787	-0.318	-0.502	-0.5960	0.0021	-0.0132

An important physical consequence of the non-trivial topological band structure is the existence of Dirac like surface states with chiral spin texture. The X points in the bulk BZ are projected to $\bar{\Gamma}$ and $\bar{X}$ points in the (001) surface BZ as shown in Fig.1(b). To study the surface state and the spin texture near $\bar{\Gamma}$ point, we consider a thick slab limited in $z \in [-d/2, d/2]$ with open boundary conditions, where d is the thickness of the slab in z direction. Now k_z is not a good quantum number which

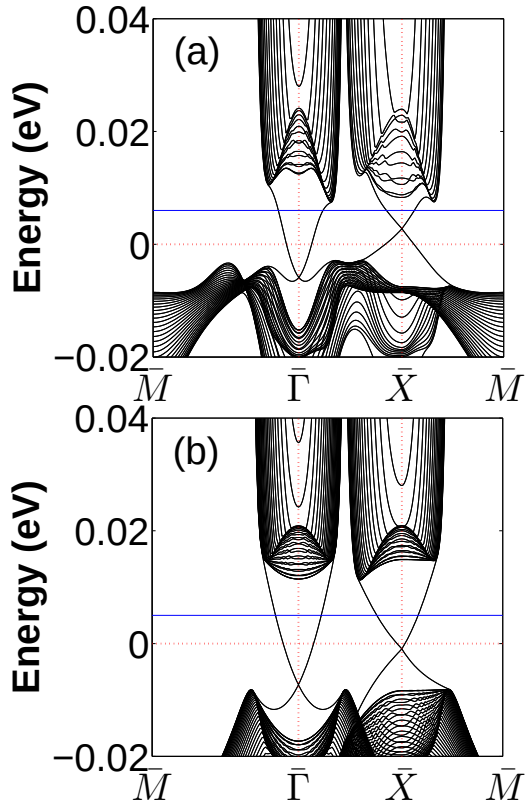

FIG. 3. The (001) direction surface states near $\bar{\Gamma}$ and $\bar{X}$ point, (a) from the tight-binding model; (b) from the k·p model results. The blue solid line indicates the energy for the spin-texture calculations.

should be replaced by $-i\partial_z$. The eigenwave function will be given by $\psi(k_x, k_y, z)$, which can be expanded using basis $\{\varphi_n(z) = \sqrt{2/d}\ sin[n\pi(z + \frac{d}{2})/d]\}$ $(n = 0, 1, 2, 3, ...)$. The Hamiltonian for the slab structure is written as $H^{slab}_{\bar{\Gamma},mn}(k_x, k_y) = \langle\varphi_m(z)|H_s(k_x, k_y, -i\partial_z)|\varphi_n(z)\rangle$. The surface states near $\bar{\Gamma}$ point can be calculated directly from $H^{slab}_{\bar{\Gamma}}(k_x, k_y)$. For the surface states and spin texture near $\bar{X}$ point, we can use the same method but change the z direction to x direction. The calculated surface states near $\bar{\Gamma}$ and $\bar{X}$ points are shown in Fig.3(b) and compared with the results from tight-binding calculation Fig.3(a). There are three Dirac cone like surface states. One located at $\bar{\Gamma}$ points, the other two located at two $\bar{X}$ points, which is different with most of the known 3D topological insulators, such as Bi_2Se_3.

From $H^{slab}_{\bar{\Gamma},\bar{X}}$ we can further get the spin texture of the surface states near $\bar{\Gamma}$ and $\bar{X}$ points. The spin texture at the energy of 6meV is shown in Fig.4, which shows a strong spin-moment locking on the surface states. We will discuss the spin texture from the symmetry consideration below.

To understand the spin orientation on the surface states, we can construct the surface effective Hamiltonian at $\bar{\Gamma}$ and $\bar{X}$ points on the 2D projected surface BZ. On the 2D BZ, the little group is C_{4v} at $\bar{\Gamma}$ point and C_{2v} at $\bar{X}$ point. The surface states at these two points are transformed as the states with $j_z = \pm 3/2$ under the symmetry operation in the little group. Form the symmetry consideration, we can write down the effective Hamiltonian for the surface states at $\bar{\Gamma}$ and $\bar{X}$ points respectively:

1) At $\bar{\Gamma}$ point: The Hamiltonian satisfy the C_{4v} symmetry and time-reversal symmetry must having the following form up to the third order of k:

$$H^{ss}_{\bar{\Gamma}}(k) = c_0k^2 + \Big[i(c_1k_+ + c_2k_+^2k_- + c_3k_-^3)\hat{\sigma}_+ + h.c.\Big], \tag{11}$$

in the basis of $\{|j_z = \frac{3}{2}\rangle, |j_z = -\frac{3}{2}\rangle\}$. Where $\hat{\sigma}_\pm = \hat{\sigma}_x \pm i\hat{\sigma}_y$, $k_\pm = k_x \pm ik_y$ and $k^2 = k_x^2 + k_y^2$. The parameters are listed in table.II

Here we should determine the spin operators $\hat{s}_{x,y,z}$ for the surface model Hamiltonian at $\bar{\Gamma}$ point . We start from the tight-binding Hamiltonian H_{eff}, which is written in the tight-binding basis space expanded by d and f orbitals located on Sm atoms. Based on this tight-binding model we can construct a thick slab terminated in the (001) direction and calculate the surface states $|\Psi_\alpha\rangle$, $\alpha = 1, 2$. The spin operator $\hat{\mathbf{S}}$ for this slab system can be easily written in the tight-binding basis. Then, we project the spin operator $\hat{\mathbf{S}}$ onto the surface states subspace. Finally, we find that the spin operators for surface states are

$$\begin{aligned} s_x^{\alpha\beta} &= \langle\Psi_\alpha|\hat{S}_x|\Psi_\beta\rangle = 0.0953\sigma_x^{\alpha\beta} \\ s_y^{\alpha\beta} &= \langle\Psi_\alpha|\hat{S}_y|\Psi_\beta\rangle = -0.0953\sigma_y^{\alpha\beta} \\ s_z^{\alpha\beta} &= \langle\Psi_\alpha|\hat{S}_z|\Psi_\beta\rangle = 0.0638\sigma_z^{\alpha\beta} \end{aligned} \tag{12}$$

The total angular momentum operators in the surface states subspace can also be calculated as $\hat{j}_x = -0.6648\hat{\sigma}_x$, $\hat{j}_y = 0.6648\hat{\sigma}_y$ $\hat{j}_z = -0.5405\hat{\sigma}_z$.

In order to predict or understand properties of the surface states under the external magnetic field, we give the Zeeman coupling terms for surface states, which takes the following form

$$H^{ss,Z}_{\bar{\Gamma}} = \mu_B \sum_{\alpha,\beta} g_{\alpha\beta}\hat{\sigma}_\alpha B_\beta, \tag{13}$$

which is obtained by projecting the $H_{Zeeman} = \frac{\mu_B}{\hbar}(\hat{\mathbf{L}} + 2\hat{\mathbf{S}})\cdot\mathbf{B}$ term into the surface states subspace. Here $\hat{\mathbf{L}}$ and $\hat{\mathbf{S}}$ are the orbital angular momentum and spin operator of the slab system. The the non-zero matrix elements of the g factor matrix for surface states at $\bar{\Gamma}$ point are listed in table.II

2) At $\bar{X}$ point: As shown in Fig.(3), the Dirac cone has a good linear dispersion. The surface effective Hamiltonian which satisfying the C_{2v} symmetry and time-reversal symmetry must have the following form up to the second order of k in the basis of $\{|j_z = \frac{3}{2}\rangle, |j_z = -\frac{3}{2}\rangle\}$,

$$H^{ss}_{\bar{X}}(\mathbf{k}) = (\epsilon_0 + a_0k^2)\sigma_0 + \big[i(a_1k_+ + a_2k_-)\hat{\sigma}_+ + h.c.\big]. \tag{14}$$

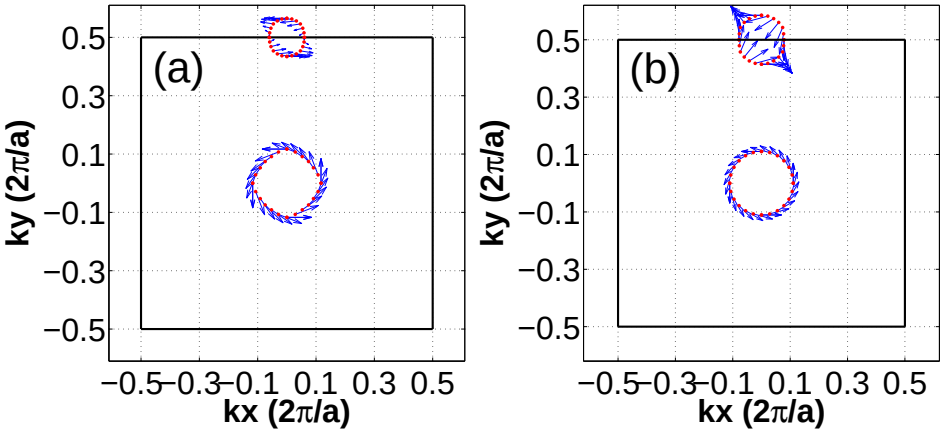

FIG. 4. Spin texture on the (001) direction surface states near $\bar{\Gamma}$ and $\bar{X}$ point, (a) from the tight-binding model; (b) from the k·p model results.

TABLE II. Parameters for the surface states model. The unit of energy is eV and the unit of length is the lattice constant.

$H^{ss}_{\bar{\Gamma}}$	c_0	c_1	c_2	c_3
	0.64105	0.01524	1.1081	-0.0516
	g_{xx}	g_{yy}	g_{zz}	
	-0.5695	0.5695	-0.4768	
$H^{ss}_{\bar{X}}$	a_0	a_1	a_2	ϵ_0
	0.011276	0.003059	-0.02322	0.008654
	g_{xx}	g_{yy}	g_{zz}	
	-0.3514	0.6647	0.7825	

The spin operators for surface states are

$$\hat{s}_x = 0.0687\hat{\sigma}_x;\ \hat{s}_y = -0.1223\hat{\sigma}_y;\ \hat{s}_z = -0.1484\hat{\sigma}_z \quad (15)$$

The total angular momentum operators in the surface states subspace can also be calculated as $\hat{j}_x = -0.4201\hat{\sigma}_x$, $\hat{j}_y = 0.7870\hat{\sigma}_y$ $\hat{j}_z = 0.9309\hat{\sigma}_z$, The Zeeman term for surface states at $\bar{X}$ point is the same as Eq.(13) and the g factors are listed in table.II.

CONCLUSIONS

To summarize, we have derived the model Hamiltonians around the three X points for the 3D TI SmB_6 based on the first principles results and the symmetry considerations. The bulk band structure, the surface states on (001) surface and the spin texture of the surface states can be well described by our model Hamiltonians. These effective Hamiltonians could facilitate further investigations of similar intriguing materials.

Acknowledgments This work was supported by the WPI Initiative on Materials Nanoarchitectonics, and Grant-in-Aid for Scientific Research under the Innovative Area "Topological Quantum Phenomena" (No.25103723), MEXT of Japan. H.M. Weng, Zhong Fang and X. Dai acknowledge the NSF of China and the 973 Program of China (No. 2011CBA00108 and No. 2013CB921700) for support.

* Hu.Xiao@nims.go.jp; daix@aphy.iphy.ac.cn

[1] X.-L. Qi and S.-C. Zhang, Reviews of Modern Physics **83**, 1057 (2011).
[2] M. Z. Hasan and C. L. Kane, Reviews of Modern Physics **82**, 3045 (2010).
[3] P. Roushan, J. Seo, C. V. Parker, Y. S. Hor, D. Hsieh, D. Qian, A. Richardella, M. Z. Hasan, R. J. Cava, and A. Yazdani, Nature **460**, 1106 (2009).
[4] Z. Alpichshev, J. G. Analytis, J.-H. Chu, I. R. Fisher, Y. L. Chen, Z. X. Shen, A. Fang, and A. Kapitulnik, Physical Review Letters **104**, 016401 (2010).
[5] T. Zhang, P. Cheng, X. Chen, J.-F. Jia, X. Ma, K. He, L. Wang, H. Zhang, X. Dai, Z. Fang, et al., Physical Review Letters **103**, 266803 (2009).
[6] Y. Xia, D. Qian, D. Hsieh, L. Wray, A. Pal, H. Lin, A. Bansil, D. Grauer, Y. S. Hor, R. J. Cava, et al., Nature Physics **5**, 398 (2009).
[7] H. Beidenkopf, P. Roushan, J. Seo, L. Gorman, I. Drozdov, Y. S. Hor, R. J. Cava, and A. Yazdani, Nature Physics **7**, 939 (2011).
[8] L. Fu and C. L. Kane, Physical Review Letters **100**, 096407 (2008).
[9] L. Santos, T. Neupert, C. Chamon, and C. Mudry, Physical Review B **81**, 184502 (2010).
[10] X.-L. Qi, T. L. Hughes, and S.-C. Zhang, Physical Review B **82**, 184516 (2010).
[11] J. E. Moore, Nature **464**, 194 (2010).
[12] M. Dzero, K. Sun, V. Galitski, and P. Coleman, Physical Review Letters **10**, 106408 (2009).
[13] M. Dzero, K. Sun, P. Coleman, and V. Galitski, Physical Review B **85**, 045130 (2012).
[14] V. Alexandrov, M. Dzero, and P. Coleman, Physical Review Letters **111**, 226403 (2013).
[15] M. Ye, J. W. Allen, and K. Sun, arXiv.org p. 7191 (2013),

1307.7191.
[16] M. Dzero and V. Galitski, Journal of Experimental and Theoretical Physics **117**, 499 (2013).
[17] F. Lu, J. Zhao, H. Weng, Z. Fang, and X. Dai, Physical Review Letters **110**, 096401 (2013).
[18] H. Weng, J. Zhao, Z. Wang, Z. Fang, and X. Dai, Physical Review Letters **112**, 016403 (2014).
[19] X. Deng, K. Haule, and G. Kotliar, Physical Review Letters **111**, 176404 (2013).
[20] V. Alexandrov, M. Dzero, and P. Coleman, Physical Review Letters **111**, 226403 (2013).
[21] M. Legner, A. Ruegg, and M. Sigrist, Physical Review B **89**, 085110 (2014).
[22] J. Werner and F. F. Assaad, Physical Review B **88**, 035113 (2013).
[23] E. Frantzeskakis, N. de Jong, B. Zwartsenberg, Y. Huang, Y. Pan, X. Zhang, J. Zhang, F. Zhang, L. Bao, O. Tegus, et al., Physical Review X **3**, 041024 (2013).
[24] S. Wolgast, Ç. Kurdak, K. Sun, J. W. Allen, D.-J. Kim, and Z. Fisk, Physical Review B **88**, 180405 (2013).
[25] N. Xu, X. Shi, P. K. Biswas, C. E. Matt, R. S. Dhaka, Y. Huang, N. C. Plumb, M. Radovic, J. H. Dil, E. Pomjakushina, et al., Physical Review B **88**, 121102 (2013).
[26] G. Li, Z. Xiang, F. Yu, T. Asaba, B. Lawson, P. Cai, C. Tinsman, A. Berkley, S. Wolgast, Y. S. Eo, et al., arXiv.org p. 5221 (2013), 1306.5221.
[27] M. Neupane, N. Alidoust, S. Y. Xu, T. Kondo, Y. Ishida, D. J. Kim, C. Liu, I. Belopolski, Y. J. Jo, T. R. Chang, et al., Nature Communications **4** (2013).
[28] D. J. Kim, S. Thomas, T. Grant, J. Botimer, Z. Fisk, and J. Xia, Nature Scientific Reports **3**, 3150 (2013).
[29] J. Jiang, S. Li, T. Zhang, Z. Sun, F. Chen, Z. R. Ye, M. Xu, Q. Q. Ge, S. Y. Tan, X. H. Niu, et al., Nature Communications **4**, 3010 (2013).
[30] S. Thomas, D. J. Kim, S. B. Chung, T. Grant, Z. Fisk, and J. Xia, arXiv.org p. 4133 (2013), 1307.4133.
[31] M. M. Yee, Y. He, A. Soumyanarayanan, D.-J. Kim, Z. Fisk, and J. E. Hoffman, arXiv.org p. 1085 (2013), 1308.1085.
[32] J. D. Denlinger, J. W. Allen, J. S. Kang, K. Sun, J. W. Kim, J. H. Shim, B. I. Min, D.-J. Kim, and Z. Fisk, arXiv.org p. 6637 (2013), 1312.6637.
[33] E. Frantzeskakis, N. de Jong, B. Zwartsenberg, Y. K. Huang, Y. Pan, X. Zhang, J. X. Zhang, F. X. Zhang, L. H. Bao, O. Tegus, et al., Physical Review X **3**, 4260431 (2013).
[34] W. Ruan, C. Ye, M. Guo, F. Chen, X. Chen, G.-M. Zhang, and Y. Wang, Physical Review Letters **112**, 136401 (2014).
[35] J. D. Denlinger, J. W. Allen, J.-S. Kang, K. Sun, B.-I. Min, D.-J. Kim, and Z. Fisk, arXiv.org p. 6636 (2013), 1312.6636.
[36] E. Beaurepaire, J. P. Kappler, and G. Krill, Physical Review B **41**, 6768 (1990).
[37] R. L. Cohen, M. Eibschutz, and K. W. West, Physical Review Letters **24**, 383 (1970).
[38] M. Eibschutz, R. L. Cohen, E. Buehler, and J. H. Wernick, Physical Review B **6**, 18 (1972).
[39] J. N. Chazalviel, M. Campagna, G. K. Wertheim, and P. H. Schmidt, Physical Review B **14**, 4586 (1976).
[40] C. L. Kane and E. J. Mele, Physical Review Letters **95**, 146802 (2005).
[41] L. Fu and C. Kane, Physical Review B **74**, 195312 (2006).
[42] X. Deng, L. Wang, X. Dai, and Z. Fang, Physical Review B **79**, 075114 (2009).
[43] G. Kotliar, S. Savrasov, K. Haule, V. Oudovenko, O. Parcollet, and C. Marianetti, Reviews of Modern Physics **78**, 865 (2006).
[44] J. KuneÅ¡, R. Arita, P. Wissgott, A. Toschi, H. Ikeda, and K. Held, Computer Physics Communications **181**, 1888 (2010).
[45] I. V. Solovyev, Z. V. Pchelkina, and V. I. Anisimov, Physical Review B **75**, 045110 (2007).
[46] A. A. Mostofi, J. R. Yates, Y.-S. Lee, I. Souza, D. Vanderbilt, and N. Marzari, Computer Physics Communications **178**, 685 (2008).